Journal of Nuclear Materials 438 (2013) S155–S159

Contents lists available at SciVerse ScienceDirect

Journal of Nuclear Materials

journal homepage: www.elsevier.com/locate/jnucmat

Splashing and boiling mechanisms of melt layer losses of PFCs during plasma instabilities

G. Miloshevsky *, A. Hassanein

Center for Materials Under Extreme Environment, School of Nuclear Engineering Purdue University, West Lafayette, IN 47907, USA

ARTICLE INFO

Article history:
Available online 11 January 2013

ABSTRACT

Due to excellent thermo-mechanical properties, tungsten (W) is considered as a promising divertor material in ITER, full divertor in JET, first wall in DEMO and ASDEX Upgrade. During plasma disruptions and ELMs the W material can be severely damaged because of macroscopic melt losses resulting in short lifetime and plasma contamination. Therefore, understanding the underlying forces and physical mechanisms of the development, motion, and removal of melt W layers is very important for successful operation of fusion devices. We have performed viscous stability analysis to assess the initial conditions for the development and growth of surface waves at the plasma-liquid W interface and computational modeling to predict the effects of viscosity, heat conduction, and phase change on the stability of melt layer. The developed theory and computational models are applicable to various fusion devices including ITER, DEMO, and current devices such as JET, TEXTOR and ASDEX.

1. Introduction

The flow of hot plasma affects tokamaks plasma-facing components (PFCs) during plasma disruptions and edge-localized modes (ELMs) [1]. The expected energy fluxes can be intense to cause rapid heating, melting, and surface vaporization of wall materials. These processes can result in severe erosion of PFCs predicted using HEIGHTS simulation package [2]. Surface erosion can even be significantly greater due to eventual macroscopic melt layer losses compared to only vaporization [3]. Recent TEXTOR experiments have shown constantly present fine melt spray and macroscopic losses of melt in the form of rare splashes with continuous ligaments and large droplets [4–6].

The inviscid stability analysis was previously used to assess the initial conditions for development and growth of surface waves at the plasma-liquid metal interface [7–9]. The computational modeling was also performed [7,8]. It is predicted that plasma streams with velocities of $\sim$100 km/s and number densities $\sim 6 \times 10^{20}$ m^{-3} can generate the growth of surface disturbances on a thin melt layer with the most unstable wavelength $\sim$2 mm that is several times larger compared to the expected melt thickness $\lesssim$0.4 mm for disruptions and giant ELMs [7]. The main computational result is observation of continuous liquid W ligaments, their elongation by the plasma flow and development of long, thin threads that can eventually break into liquid droplets [8].

In this work, the inviscid stability theory [7–9] is further developed to include the effects of viscosity, heat transfer, and mass exchange across the interface [10,11]. The critical velocity as a function of wavelength is analyzed for various values of plasma viscosity and heat transfer coefficient. The CFD solver that includes the heat transfer and vaporization effects is developed using the open-source OpenFoam CFD libraries [12]. The effects of heat conduction and phase change on melt layer stability are computationally studied.

2. Melt layer stability analysis and computational model

The effects of viscosity, mass exchange, and heat transfer across the interface can significantly influence melt layer stability, especially when the melt is boiling with bubble bursts [13]. We have adapted the approach of viscous potential flow developed by Funada and Joseph [10]. The problem of flow with mass and heat transfer in the stability analysis is considered using simplified formulation of Hsieh [11]. Using harmonic normal modes in the linearized Navier-Stock equations, we derive the expression for the relative velocity $\Delta V = |V_p - V_m|$ of the viscous instability [10,14]

* Corresponding author. Address: 400 Central Drive, West Lafayette, IN 47907-2017, USA.
E-mail addresses: gennady@purdue.edu (G. Miloshevsky), hassanein@purdue.edu (A. Hassanein).

0022-3115/$ - see front matter © 2013 Elsevier B.V. All rights reserved.
http://dx.doi.org/10.1016/j.jnucmat.2013.01.024

$$\Delta V > \sqrt{\frac{2(\delta(\coth(kh_m)+\coth(kh_p))+2k^2(\mu'_m+\mu'_p))^2\times[(kg(\rho_m-\rho_p)+k^3(\sigma+\sigma_H))/(2k^2)+\delta(\mu'_m/\rho_m+\mu'_p/\rho_p)]}{\delta^2(\rho'_p\coth^2(kh_m)+\rho'_m\coth^2(kh_p))+4k^4(\rho'_m\mu'^2_p+\rho'_p\mu'^2_m)+4\delta k^2(\rho'_p\mu'_m\coth(kh_m)+\rho'_m\mu'_p\coth(kh_p))}} \quad (1)$$

where V_j, ρ_j are velocity and mass density, $\rho'_j=\rho_j\coth(kh_j)$, $\mu'_j=\mu_j\coth(kh_j)$, μ_j and h_j are viscosity and thickness of plasma and melt with $j=p,m$, $k=2\pi/\lambda$ is wave number associated with small disturbances $\sim\exp(i(kx+\omega t))$, λ is wavelength, ω is frequency, g is gravity constant, σ and σ_H are interfacial and magnetic tension, $\delta=(1/h_m-1/h_p)F/L$ is coefficient of heat transfer, L is latent heat of evaporation, $F=-K(T_m-T_i)/h_m$ is equilibrium heat flux, K is heat conduction coefficient, T_i and T_m are interface and melt temperature. The definition of σ_H can be found in [7]. This viscous stability analysis with account of heat transfer and phase change was applied to the plasma-W melt.

The Volume of Fluid (VOF) approach [7] is used to track the interface. A transport equation for the volume fraction of melt phase α_m can be written as

$$\frac{\partial\alpha_m}{\partial t}+\nabla\cdot(\alpha_m\vec{u})+\nabla\cdot(\alpha_m(1-\alpha_m)\vec{u}_c)=\frac{\dot{m}}{\rho} \quad (2)$$

where $\vec{u}$ is single velocity field, $\rho=\alpha_m\rho_m+\alpha_p\rho_p$ is density field assuming values of ρ_m and ρ_p for melt and plasma phases, $\alpha_p=1-\alpha_m$ is volume fraction of plasma, $\dot{m}$ is mass transfer rate of molten W due to vaporization at the interface, and $\vec{u}_c$ is compression velocity which is included for artificial interface compression. This extra compression contributes only in interfacial region providing sharp interface and ensuring that α_m is limited between 0 and 1. We assume that evaporated W contributes to the plasma state since its fraction is small. The mass conservation equation is given as

$$\frac{\partial\rho}{\partial t}+\nabla\cdot(\rho\vec{u})=\dot{m} \quad (3)$$

where $\dot{m}$ is a source term due to the phase change. The momentum equation can be written as

$$\frac{\partial\rho\vec{u}}{\partial t}+\nabla\cdot(\rho\vec{u}\vec{u})=-\nabla p+\nabla\cdot(\mu(\nabla\vec{u}+(\nabla\vec{u})^T))+\sigma\kappa\nabla\alpha_m+\rho\vec{g} \quad (4)$$

where p is single pressure field, $\mu=\alpha_m\mu_m+\alpha_p\mu_p$ is viscosity with components of μ_m and μ_p for W-melt and plasma phase, $\kappa=-\nabla\cdot(\nabla\alpha_m/|\nabla\alpha_m|)$ is curvature of the interface. The gravity $\vec{g}$ is included as a body force. The equation of thermal energy is given by

$$\frac{\partial\rho c_pT}{\partial t}+\nabla\cdot(\rho c_p\vec{u}T)=\nabla\cdot(K\nabla T)+\dot{h} \quad (5)$$

where T is single temperature field, $c_p=\alpha_mc_{pm}+\alpha_pc_{pp}$ and $K=\alpha_mK_m+\alpha_pK_p$ are respectively the specific heat capacity at constant pressure and thermal conductivity assuming the values c_{pm}, K_m and c_{pp}, K_p for melt and plasma phases, $\dot{h}$ is a source term accounting for enthalpy of vaporization (latent heat of phase change).

For droplet spraying at high-speed flows, the following linearized equations of state $\rho_j=\rho_{0j}+\psi_j(p-p_{0j})-\zeta_j(T-T_{0j})$ are implemented with $j=m$, p. Here ψ_j, ζ_j are the coefficients of compressibility and thermal expansion of melt and plasma, ρ_{0j}, p_{0j}, T_{0j} correspond to a reference state about which a linearization is performed. The compressibility $\psi_m\sim1/c_m^2\sim10^{-7}$ s^2/m^2 is estimated using the speed of sound $c_m=3.2$ km/s in the W-melt [15]. The thermal expansion coefficient of W-liquid is $\zeta_m\sim4.3\times10^{-5}$ 1/K [15]. The expansion and compressibility coefficients of plasma are estimated using the ideal gas law $p=\rho R_pT$ as $\zeta_p=1/T$ and $\psi_p=1/(R_pT)$ with $R_p=8248.5$ J/(kg K) is hydrogen gas constant.

We use the phase change model developed by Hardt and Wondra [16] that is suitable for continuum-field calculations and compatible with VOF approach. The evaporation mass flux density (in kg m^{-3}s^{-1}) at phase boundary is defined as $\dot{m}=(T_i-T_s)N\alpha_m\nabla\alpha_m/(R_{mv}L)$, where $T_s=5936$ K is saturation temperature at which the W-melt begins to boil. The latent heat of W vaporization is $L=4620$ kJ/kg. The heat resistance R_{mv} of W-melt-vapor plasma interface is defined as $R_{mv}=(2-\chi)T_s^{3/2}\sqrt{2\pi R_v}/(2\chi L^2\rho_v)$ [16], where $\chi=1$ is evaporation coefficient and $R_v=54.2$ J/(kg K) is the gas constant of W-vapor. For estimation of R_{mv} the vapor density ρ_v is assumed to be the same as the plasma density. A normalization factor N is determined from the equation $N\int_\Omega\alpha_m|\nabla\alpha_m|d\Omega=\int_\Omega|\nabla\alpha_m|d\Omega$, where Ω is the computational domain. In 2D, the integral over Ω gives the interface length. The source-term $\dot{h}$ in Eq. (5) can be expressed as $\dot{h}=L\dot{m}$. In current implementation, the interaction of W-vapor with W-melt and hydrogen plasma is neglected since evaporation losses are small. The inclusion of W-vapor will require the extension of the VOF model to three fluids two of which are miscible (plasma and W-vapor).

The CFD solver was developed and implemented using the OpenFoam library [12] that includes numerical solvers, preprocessing, and postprocessing routines. The thermal energy equation, heat, and vaporization models were implemented in *compressibleInterFoam*. The evaporation model was validated against the Stefan problems.

3. Theoretical and simulation results

The viscous stability analysis was applied to the plasma W-melt system shown in Fig. 1. The density of hydrogen plasma is $\sim10^{20}$ m^{-3}($\rho_p\sim1.67\times10^{-7}$ kg/m^3) relevant for ITER conditions. The plasma velocity was in the range from 1 to 100 km/s. The viscosity of plasma was varied from zero to 10^{-5} kg/(m s). The specific heat capacity is estimated using the ideal gas law as $c_{pp}=\gamma R_p/(\gamma-1)$, where $\gamma=5/3$ is the adiabatic constant of a monatomic hydrogen plasma. The thermal conductivity for a hydrogen plasma due to electrons is estimated as $K_p\sim4.4\times10^{-11}(T[K])^{5/2}(\ln\Lambda/10)^{-1}$ W/(m K), where $\ln\Lambda\sim10$ is the Coulomb logarithm. The W-melt density is $\rho_m=16{,}400$ kg/m^3. Melt thickness is ~200 μm [2]. The surface tension is $\sigma=2.48$ N/m. The velocity of melt is ~1 m/s. The viscosity of W-melt is $\mu_m\sim7\times10^{-3}$kg/(m s). The temperature of molten W is $T_m=3695$ K. The heat conduction coefficient of W-melt is $K_m\sim80$ W/(m K). The specific heat capacity of W-melt is $c_{pm}\sim280$ J/(kg K).

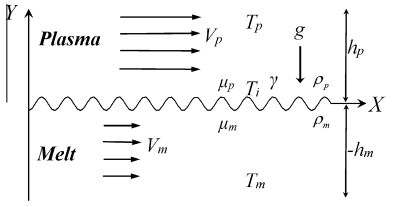

Fig. 1. Schematic illustration of the plasma-melt system.

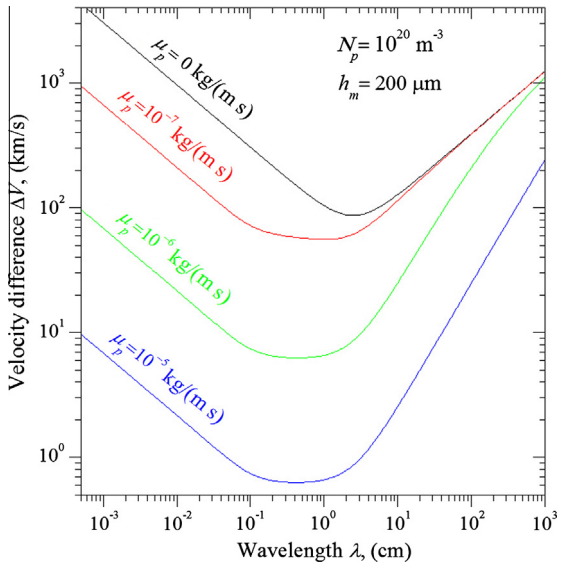

Fig. 2. The critical velocity as a function of wavelength for various values of plasma viscosity.

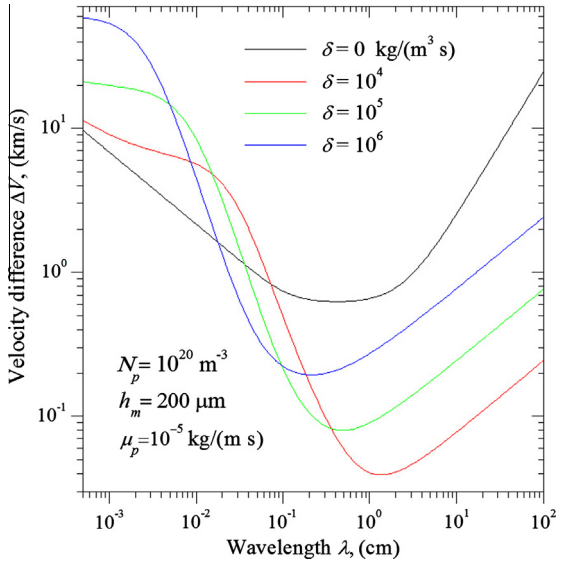

Fig. 3. Critical velocity as function of wavelength for various values of heat transfer coefficient.

The critical velocity as a function of wavelength λ is shown in Fig. 2 for various values of plasma viscosity. For viscous plasma-melt flow, the critical velocity is significantly reduced with the increase in plasma viscosity. Growing waves with $\lambda_c \sim 0.5$ cm can be generated by the viscous plasma with $\mu_p \sim 10^{-5}$ kg/(m s) and $\Delta V > 0.6$ km/s (blue curve). When the relative velocity ~10 km/s, the fastest growing "dangerous" wavelength is ~6 μm with the growth rate ~0.1 μs. A critical velocity of $\Delta V \sim 100$ km/s is required in the inviscid case to produce the instability (black curve). The value of critical wavelength λ_c is shifted slightly toward shorter wavelengths as the viscosity of plasma increases.

The influence of heat and mass transfer across plasma-melt interface on melt layer stability is demonstrated in Fig. 3. Long wavelengths are strongly destabilized due to thermal effects and the critical velocity is significantly reduced. The wavelength with maximum growth rate increases. For larger thermal flux (larger δ), the critical velocity increases approaching the case with $\delta = 0$. However, the short-length capillary waves are stabilized with increase of δ. The presence of intense heat and mass transfer can stabilize the interface against otherwise destabilizing viscosity effects on short wavelengths (blue[1] curve in Fig. 3).

The computed fields of volume fractions of plasma and melt are shown in Fig. 4. The phase change is not included with the melt experiencing only viscous and thermal stresses. The domain is 5 mm × 1 mm with the grid size of 10 μm. The melt depth is 200 μm. At the bottom of the computational domain (Fig. 4), W-melt is held at melting temperature and the plasma is hotter ($T_p \sim 4000$ K at the top of the computational domain). Plasma velocity is 10 km/s. The modeling is performed for the plasma-melt system at 10^3, 10^4 and 10^5 Pa. Faster melt destabilization is observed at higher pressures. The results are presented in Fig. 4 for 10^3 Pa relevant for ITER conditions [4]. The interface is initially perturbed with 10 (Fig. 4a), 20 (Fig. 4b), and 40 (Fig. 4c) wavelengths. The waves with shorter wavelengths grow much faster than those with longer wavelengths. At an interface perturbed with 10 wavelengths, thin protrusions are initially developed. Later, 10 large waves undergo local growth gradually transforming into ligaments (Fig. 4a). The stripping of fine droplets from wave crests and tips of ligaments is observed. The small droplets are dragged by plasma colliding with each other, merging, and creating larger droplets. The droplets merge with melt waves subsequently creating protrusions that can transform into secondary droplets (Fig. 4a). In two other cases with the interface perturbed by shorter wavelengths (Fig. 4b and c), the entrainment of plasma into the melt is observed due to plunging of wave tips onto nearby ligaments (Fig. 4b). Plasma bubbles are trapped in the melt. At times >0.1 ms, the interface represents a complex structure with droplets, melt breaks, ligaments, fingers, open shapes, and trapped plasma bubbles (Fig. 4c).

The phase-change effects on the stability of surface waves are illustrated in Fig. 5. At the bottom of the computational domain, the temperature of melt is set to the boiling (saturation) temperature with plasma temperature kept higher ($T_p \sim 6000$ K at the top of the computational domain). Fifty wavelengths were excited at the interface. The short-length waves start to grow slightly during $\lesssim 5$ μs. Afterward, the growth slows down at ~10 μs and the volume fraction of melt at wave crests is reduced. The waves disappear at ~30 μs with the interface is nearly flat even at ~150 μs. The thickness of melt is reduced due to vaporization. It should be noted that the heat flux and temperature gradients are kept constant during simulation. The plasma energy deposition and W-vapor shielding were not included. Therefore, these results demonstrate the melt stabilization, not vaporization losses.

An estimate of W melt losses using the capillary droplet model [9] based on viscous potential flow theory [10] is shown in Fig. 6. It is assumed that droplets are formed due to breakaway of melt at peaks of short waves (Fig. 4). The horizontal black line indicates the thickness of initial melt layer, $h_m = 200$ μm. For plasma streaming with velocity >15 km/s and viscosity ~10^{-5} kg/(m s), the entire melt layer can be lost during $\tau = 0.1$ ms. For smaller plasma viscosity ~10^{-6} kg/(m s), the thickness of melt ~100 μm can be removed due to plasma impact with ~100 km/s. For plasma with even smaller viscosity ~10^{-7} kg/(m s) and flowing with velocity ~65–100 km/s, the lost melt is ~0.5–4 μm.

4. Discussion

According to the stability analysis based on the viscous potential flow theory [10], the stability of melt layer is significantly

[1] For interpretation of color in Fig. 3, the reader is referred to the web version of this article.

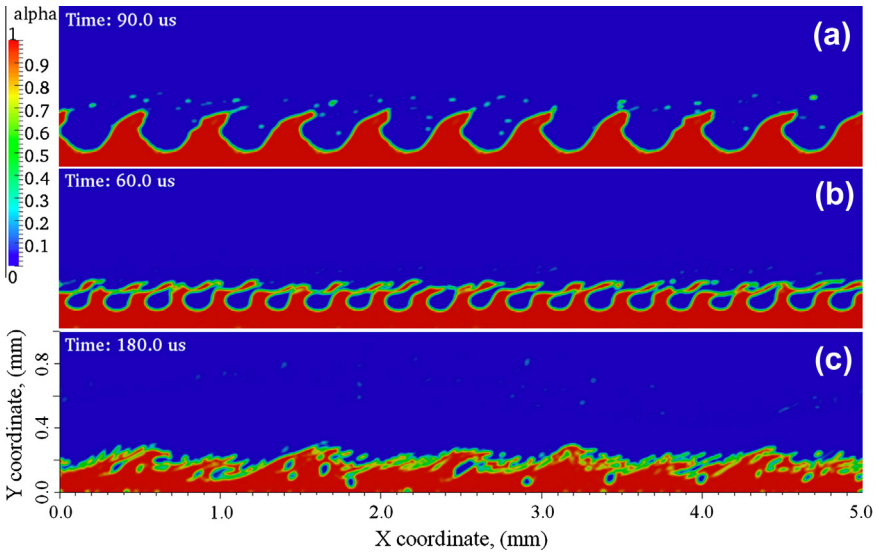

Fig. 4. Snapshots of volume fractions with the interface initially excited with (a) 10, (b) 20, and (c) 40 wavelengths. The topology of plasma-melt interface is shown at (a) 90 μs, (b) 60 μs and (c) 180 μs.

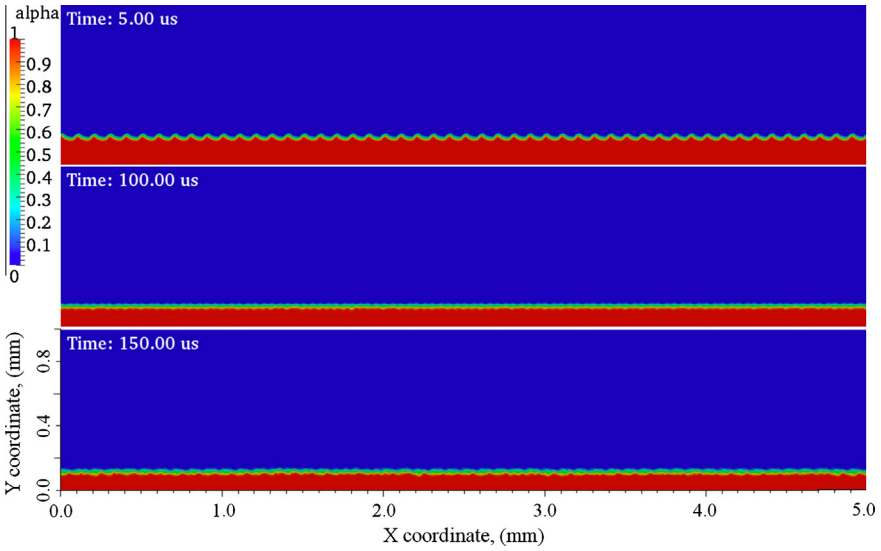

Fig. 5. Evolution of volume fractions of plasma-melt flow with phase change taking into account. The interface was initially excited with 50 wavelengths.

influenced by small but finite viscosity of plasma. We find that viscosity effects are destabilizing. Eq. (1) for critical velocity of viscous plasma-melt flow can be reduced to that of inviscid flow [7] by assigning $\delta = 0$ and $\mu_p = 0$. The inviscid formula can be also derived by replacing the ratio $m = \mu_p/\mu_m$ with $r = \rho_p/\rho_m$. In our melt problem, $m \sim 0.1$ and $r \sim 10^{-10}$ ($m \gg r$, so-called low-viscosity fluids) [10]. The variation in the stability is very large when m is larger than r [10]. Therefore ΔV is rapidly varying with variation of m (Fig. 2). The critical velocity for viscous fluids is always smaller than that for inviscid fluids. It is a maximum at $m = r$ corresponding to the inviscid case. Thus, accounting for small viscous effects completely changes the inviscid instability.

Although inertial forces prevail in high-speed bulk plasma flow, at the plasma-melt interface a thin boundary layer develops in which viscous forces are very important. Close to the interface, the plasma velocity sharply decreases from its bulk value to that of melt motion. Plasma transfers the momentum to surface melt layers due to the friction, or stickiness of real fluids. The viscous stresses can develop causing friction drag of melt. These viscous stresses are significant due to high velocity gradients in a boundary layer. Melt disturbances can grow as viscous fingers. The destabilizing suction of melt into ligaments can dominate the stabilizing effect of surface tension. Arrays of melt protrusions have been observed in our CFD modeling that did not include phase change effects. We speculate that viscous melt fingering could be relevant to regular ligament-like structures on the melt surface revealed in TEXTOR experiments [5]. The disturbances with shorter wavelengths evolve much faster than those with longer wavelengths. This finding agrees with predictions of the viscous stability analysis. Fine droplets are sprayed from the melt even in the case of waves and ligaments with large wavelength. For short-length disturbances, the viscous fingers induced at the interface quickly grow, plunge onto neighbor fingers, thus entraining plasma bubbles into the melt. A complex interface topology develops as a result of melt motion and splashing. The disintegration of melt as a whole was not observed under the modeled plasma conditions.

At high heat loads ~10–100 MJ/m^2 with load duration ~0.1–10 ms (plasma disruptions), rapid vaporization can take place at

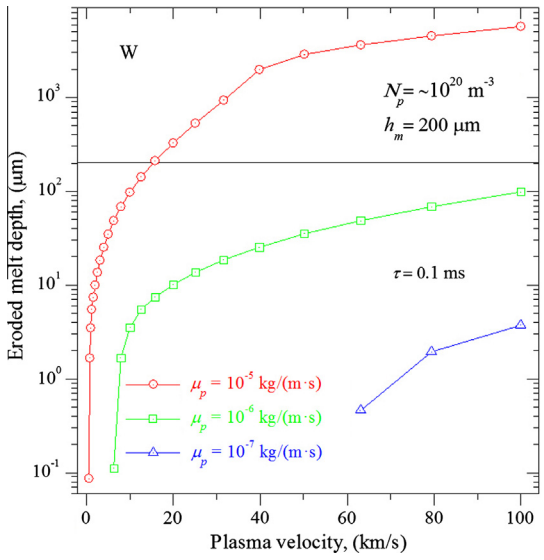

Fig. 6. Thickness of removed W melt during $\tau = 0.1$ ms as a function of the plasma velocity for different values of plasma viscosity.

the surface of the melt. We find that the phase change with heat and mass transfer across the interface suppresses the development and growth of short-length waves. The pressure and viscous stresses facilitate the instability, but heat and mass transfer effects stabilize the interface. The melt crests evaporate locally since they are closer to the hotter plasma than melt troughs. This phenomenon flattens the interface with an evaporation front moving into the melt. The formation of vapor bubbles in melt is not observed since the nucleation model is not included.

The viscous stability analysis and CFD modeling have revealed that viscous plasma flowing over melt surface with velocities >10 km/s can generate growing waves in the 1–10 μm wavelength range. This wavelength is much smaller compared to the thickness of melt ~200 μm making the capillary droplet model [9] applicable for estimations of melt losses. The estimates show that high-viscosity plasma $\sim 10^{-5}$ kg/(m s) streaming with high speeds >10 km/s is capable of eroding melt layers with thickness larger than ~200 μm .

Effects of magnetic field on melt stability are also investigated using Eq. (1). As in an inviscid case [7], W-melt is stable for the plasma streaming along the magnetic lines (toroidal direction), and no stabilization is predicted for the plasma flowing perpendicular to the magnetic lines (poloidal direction). However, it is found that melt stabilization is much weaker in the toroidal direction compared to an inviscid case [7]. The melt can be destabilized by the viscous plasma flowing with velocity ~50 km/s along the magnetic field with ~5 T. The results on stability curves are not shown due to space limitations. The magnetic field is not yet implemented in the VOF model. We presume that our computational results are correct for the plasma flowing in the poloidal direction.

5. Summary

Stability analysis based on the viscous potential flow theory and accounting for heat and mass transfer across the interface is used to study plasma-melt instability. It is predicted that viscous normal stress at the interface has destabilizing effect on melt layers. The critical velocity required to induce the instability is greatly reduced, and the range of fastest growing waves extends toward shorter wavelengths. However, the heat and mass transfer phenomena stabilize the short-length waves. The CFD modeling that includes effects of plasma streaming, surface tension, gravity, shear, viscous and thermal stresses, heat and mass transfer is also performed. In the absence of melt evaporation, the main observations are the growth of short-length waves, their transformations into ligaments with fine melt droplets continuously stripped from ligament tips and dragged away by the plasma flow. Melt losses are estimated for ITER conditions using the capillary droplet model. In the presence of intense phase change at the interface under the same flow conditions as used before, it is found that the growth of unstable waves is suppressed and melt is stabilized. It is important to point out that further investigations are needed to quantify this viscosity-induced instability, stress disturbances in the melt layer, and melt stabilization due to heat and mass transfer.

Acknowledgements

This work is supported by the U.S. Department of Energy, Office of Fusion Energy Sciences. TeraGrid computational resources provided by the NCSA under Grant TG-PHY090096.

References

[1] G. Federici, C.H. Skinner, J.N. Brooks, et al., Nucl. Fusion 41 (2001) 1967–2137.
[2] A. Hassanein, I. Konkashbaev, J. Nucl. Mater. 273 (1999) 326–333.
[3] A. Hassanein, I. Konkashbaev, J. Nucl. Mater. 233–237 (1996) 713–717.
[4] J.W. Coenen, B. Bazylev, S. Brezinsek, et al., J. Nucl. Mater. 415 (2011) S78–S82.
[5] J.W. Coenen, V. Philipps, S. Brezinsek, et al., Nucl. Fusion 51 (2011) 083008.
[6] J.W. Coenen, V. Philipps, S. Brezinsek, et al., Nucl. Fusion 51 (2011) 113020.
[7] G.V. Miloshevsky, A. Hassanein, Nucl. Fusion 50 (2010) 115005.
[8] G. Miloshevsky, A. Hassanein, J. Nucl. Mater. 415 (2011) S74–S77.
[9] Y. Shi, G. Miloshevsky, A. Hassanein, J. Nucl. Mater. 412 (2011) 123–128.
[10] T. Funada, D.D. Joseph, J. Fluid Mech. 445 (2001) 263–283.
[11] D.Y. Hsieh, Phys. Fluids 21 (1978) 745–748.
[12] OpenFOAM, user guide, version 2.1. <http://www.openfoam.org>, 2012.
[13] Y. Shi, G.V. Miloshevsky, A. Hassanein, Fusion Eng. Des. 86 (2011) 155–162.
[14] R. Asthana, G.S. Agrawal, Physica A 382 (2007) 389–404.
[15] A.D. Rakhel, A. Kloss, H. Hess, Int. J. Thermophys. 23 (2002) 1369–1380.
[16] S. Hardt, F. Wondra, J. Comput. Phys. 227 (2008) 5871–5895.